A Slowly Inactivating Potassium Current Truncates Spike Activity in Ganglion Cells of the Tiger Salamander Retina

Peter Lukasiewicz and Frank Werblin

Neurobiology Group, University of California, Berkeley, California 94720

Voltage-gated ganglion cell membrane currents were studied under whole-cell patch clamp in isolation and in retinal slices. The cells were identified by (1) backfilling their axons with rhodamine and later identifying them by their fluorescence in the slice or the mix of isolated cells or (2) by filling them with Lucifer yellow during recording in retinal slices. Both methods yielded cells with similar currents. In some cases, isolated cells lacked processes yet showed currents similar to other cells, suggesting that voltage-gated currents in all cells were located primarily at the soma. Both a conventional inactivating sodium current and a sustained calcium current were found.

We describe 3 inactivating outward currents, ordered in their rate of inactivation. The fastest current resembled I_A reported by Connor and Stevens (1971a, b). A slower current labeled I_B inactivated with a time constant of 339 msec at 0 mV. The current with slowest inactivation is labeled I_C here, inactivating with a time constant of 4.03 sec at 0 mV. An additional outward current was sustained and calcium dependent, labeled $I_{K(Ca)}$.

I_B was the largest of these currents. It was slower than I_A, was not blocked by 4AP, and inactivated over a much more positive potential range. I_B appears to play an important role in spike generation, different from that of I_A: Its inactivation leads to a slow depolarizing shift of the membrane during a current step, truncating spike activity after about 300–700 msec as the membrane potential enters the region of sodium inactivation. We analyze how the inactivating outward current acts to ensure a graded spiking response and to truncate the spiking output in the presence of large excitatory inputs.

The modulation of spiking in ganglion cells is controlled by the interaction of synaptic and voltage-gated currents. In lower vertebrates, various synaptic inputs converge upon ganglion cells to mediate different forms of response (Miller and Dacheux, 1976; Baylor and Fettiplace, 1979; Wunk and Werblin, 1979; Belgum et al., 1982, 1983). Little is known about the role of voltage-gated currents in the ganglion cell membrane in modulating spike activity. Baylor and Fettiplace (1979) showed that in turtle the ganglion cell membrane voltage and spike frequency were linear with input current over a major part of the physiological range. However, since recent patch recordings indicate

a significantly higher input resistance in ganglion cells, the leak caused by conventional intracellular electrodes might have shunted the membrane in those measurements so that nonlinear events mediated by voltage-gated currents could have gone unnoticed.

We have studied the voltage-gated ganglion cell currents, both in isolated cells and in retinal slices, to determine the nature of the interactions that might modulate spike activity. Most currents were quite conventional and similar to those described by Lipton and Tauck (1987) in isolated rat ganglion cells. A large, slowly inactivating outward current appears to control the magnitude and duration of spiking. Preliminary reports have appeared elsewhere (Lukasiewicz and Werblin, 1985, 1986).

Materials and Methods

Preparation. Whole-cell patch recordings (Hamill et al., 1981) were made from ganglion cells in the retinal slice and in isolated cells. Retinal slices were prepared using procedures described by Werblin (1978). Briefly, the vitreal side of a small piece of retina was placed against a Millipore filter. The sclera was then pulled away, leaving the retina adhering to the filter. The filter and retina were then sliced with a razorblade at 150 μm intervals and positioned so that all the cells spanning the sliced edge could be viewed under a Zeiss 40× water-immersion objective. The slices were held in place by embedding the ends of the Millipore filter, which extended well beyond the retina, in Vaseline.

Isolated cells were prepared using the methods of Firestein and Werblin (1987). Briefly, retinas were isolated and incubated in a Ringer solution containing 1 mg/ml papain (Sigma, St. Louis) and 0.5 mg/ml N-acetyl-L-cysteine (Sigma) for 30 min at 30°C. The tissue was transferred to a 5% bovine serum solution for 10 min to quench residual papain activity. After several washes in Ringer, the digested retinas were gently triturated with pasteur pipettes to isolate the cells.

Cell identification. Cells in the slice and in isolation were visualized using Hoffman modulation contrast optics (Modulation Optics, Inc., Greenvale, NY). Ganglion cells were identified, using Lucifer yellow (Stewart, 1978), by the characteristic ramification of their processes within the inner plexiform layer and by the presence of axons.

Isolated cells were identified after being backfilled with rhodamine. Initially, several crystals of tetramethylrhodamine isothiocyanate, isomer R (RITC) (Sigma) were applied, after decapitation, to the distal end of the optic nerve. Following incubation of the head for 18–24 hr at 5°C, cells were isolated as described above (Preparation). Cells that were fluorescent in the isolated mix were taken to be ganglion cells. In slice preparations prepared after the same incubation, almost all cells in the ganglion cell layer and virtually no cells in other layers were fluorescent (see Fig. 1). On rare occasions a singular cell, most likely a displaced ganglion cell, was stained in the inner nuclear layer. This shows that there was no significant leakage of rhodamine between adjacent cells.

Bathing solutions. Amphibian Ringer, pH 7.7–7.8, bathed the slices or isolated cells; the composition of this and the other solutions used to perfuse the slice are listed in Table 1. In some cases excessive spontaneous inhibitory activity was encountered, requiring that strychnine and picrotoxin (50 μM) be added to the bathing media to block this activity. No cells used in the figures shown here had such spontaneous activity. Tetrodotoxin (TTX; 0.3–1 μM) was added directly to the bathing solutions without substitution.

Table 1. Composition of bathing solutions (in mM)

Component	A Control	B Sodium isolation	C $I_{(Ca)}/I_{(K)}$ isolation	D I_B/I_C isolation	E I_A isolation
NaCl	120	120	120	120	100
TEA	0	0	0	0	20
KCl	2	2	2	2	2
CaCl$_2$	4	0	4	0	0
CoCl$_2$	0	2	0	2	2
Glucose	3	3	3	3	3
HEPES	5	5	5	5	5
TTX	0	0	0.001	0.001	0.001

The solution bathing the slice was changed using a multichannel perfusion pump. The volume of the experimental chamber was 1 ml, and the flow rate was 0.2–0.4 ml/min, so the bulk of the solution could be exchanged in about 2 min. Solutions were introduced through a pipette with 5 μm tip diameter placed near the slice so the solution around the slice was exchanged first.

Electrode solutions. Potassium or cesium and TEA were the predominant cations contained in the patch electrode solutions. The complete composition of the solutions contained in the electrodes is listed in Table 2. In about 25% of the work, 2 mM Mg^{2+} was added to the electrode solution and Ca^{2+} concentration was reduced to 10^{-9} M. Experiments were performed at room temperature (20–24°C).

Liquid junction potential correction. Liquid junction potentials were determined by first placing the electrodes in a bath containing the electrode solution to establish a zero offset potential. Then, we measured the offset from the zero potential in normal bathing media. The offset was 3 mV at 120 mM Cl$^-$ and 96 mM Cs$^+$/20 mM TEA$^+$, 4 mV at 120 mM Cl$^-$ and 116 mM K$^+$. Membrane potential values in this paper are corrected for these junction potentials.

Electrical constants of the membrane. Measurements for determining membrane resistance, capacitance, and resting level are shown in Figure 2. Figure 2A shows a voltage response to a 10 pA depolarizing current. The potential change evoked did not activate any voltage-gated currents (see below). The charging curve has a time constant of 20.0 msec. The plateau potential is 13.4 mV, so the membrane capacitance is 15.1 pF. We consistently measured input resistances averaging about 3 GΩ, nearly an order of magnitude larger than previously reported using intracellular recording (Werblin, 1977; Baylor and Fettiplace, 1979). In some cells, the resting potential was initially around −40 mV but became more negative during the experiment, reaching a steady value similar to that derived from intracellular recording (mean, −67.5 mV, 41 cells). Statistics from all such measurements are summarized in Table 3.

Ganglion cells can have extensive dendritic fields extending up to 200 μm from the cell body. The inability to adequately space-clamp such cells may introduce errors in the magnitude and kinetics of our measurements. Studies with enzymatically dissociated cells, often without any processes, showed similar currents, suggesting that the majority of the voltage-gated channels are located on or near the soma. The sodium

channels mediating spike activity in ganglion cells are probably also located near the cell soma (Wollner and Catterall, 1986).

Series resistance. We used the membrane capacitance of 15 pF (Fig. 2A) and the time constant of the charging curve under *voltage clamp* in Figure 2B to determine the value of the series resistance. The time constant for the charging curve in Figure 2B was 0.15 msec, giving a series resistance of about 10 MΩ. For the largest currents we measured here, near 1 nA, this series resistance would give an error of about 10 mV. Most currents were smaller, so the errors in amplitude and kinetics due to the series resistance will be small.

Recording system. Patch electrodes of 3–7 MΩ resistance in Ringer were made on a David Kopf electrode puller (David Kopf, Coalinga, CA) using borosilicate glass (TW150-4, WPI Instruments, New Haven, CT). A List L/M-EPC7 patch clamp (Medical Systems Corp., Greenvale, NY) was used to voltage-clamp and/or current-clamp ganglion cells. Filtering was at 3 kHz. Sampling rate was either 1 or 6.7 kHz, depending upon the length of the record. The responses and stimuli were digitized by a Data Translations DT2801 analog-to-digital interface and recorded on an IBM PC/XT. Preprogrammed stimuli were delivered to the command input of the patch clamp using a digital-to-analog interface.

Results

Whole-cell currents. Figure 3A shows a series of representative currents elicited from an isolated ganglion cell held at −75 mV and depolarized in 5 mV steps. A transient inward current was activated at potentials positive to −40 mV and reached a maximum value of 1.2 nA at a step to −15 mV. A sustained outward current was activated at step potentials positive to −40 mV and reached a magnitude of 380 pA at −15 mV. Similar results were obtained from 14 other cells (see Table 3).

The responses to hyperpolarizing voltage steps are shown in Figure 3B. We found no evidence for voltage-gated currents at potentials more negative than the resting level of the cell, yet horizontal cells (Lasater, 1986) and bipolar cells (Kaneko and Tachibana, 1985) appear to have these currents. The inset in Figure 3B shows that over the voltage range from −80 to −150 mV the cell had a linear conductance of 0.9 nS, or an input resistance of 1.1 GΩ. Table 3 shows the range of input resistances for all cells studied.
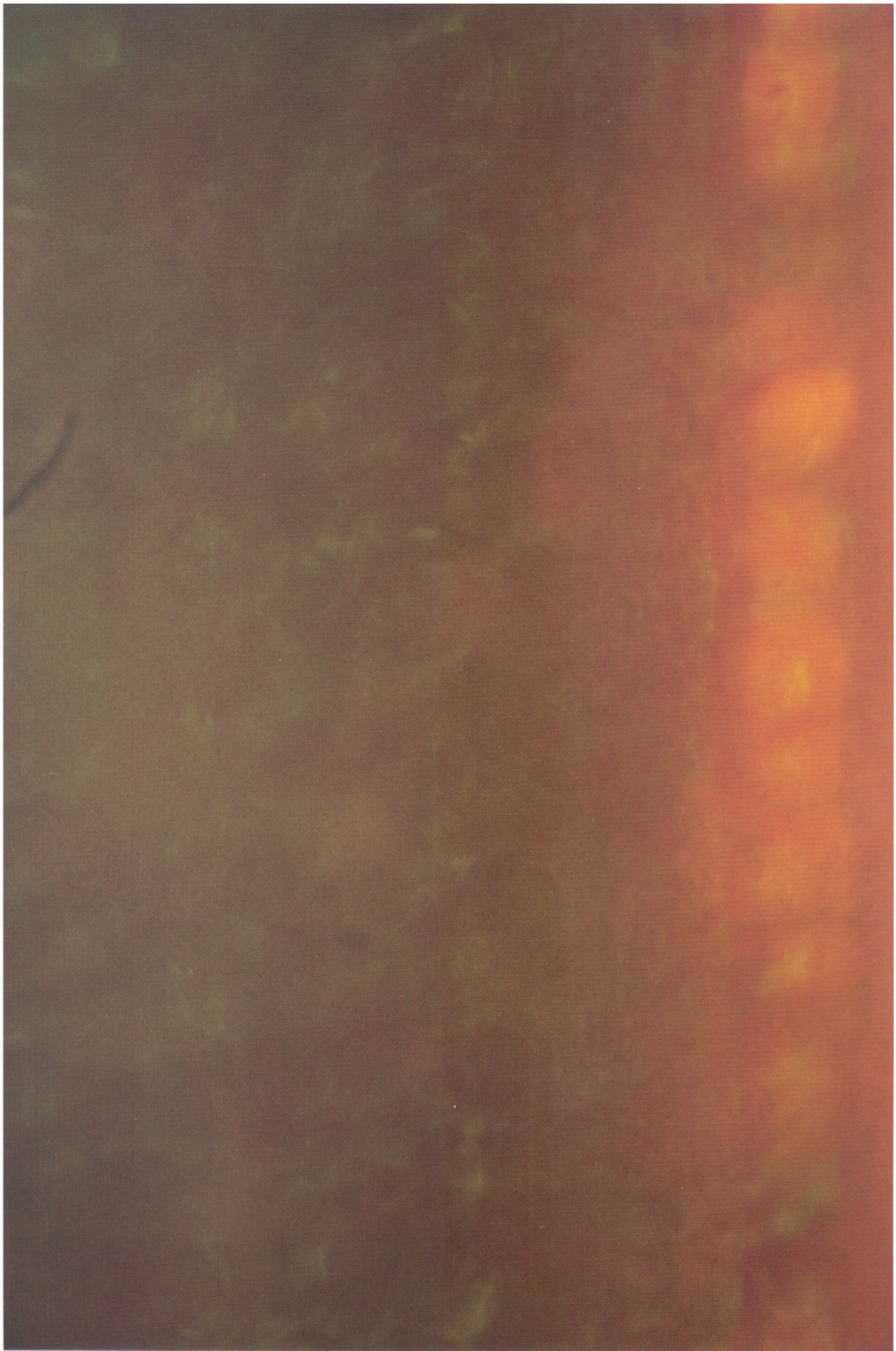
Activation of transient inward current. A transient inward current was measured in isolation by blocking the outward currents with 96 mM cesium and 20 mM TEA in the recording electrode and blocking calcium current with 2 mM cobalt replacing calcium in the bathing medium (Weakly, 1973). Twenty-one cells were studied in this way with consistent results. Figure 4A shows a series of selected inward currents elicited when the cell was held at −75 mV and depolarized to the indicated potentials.
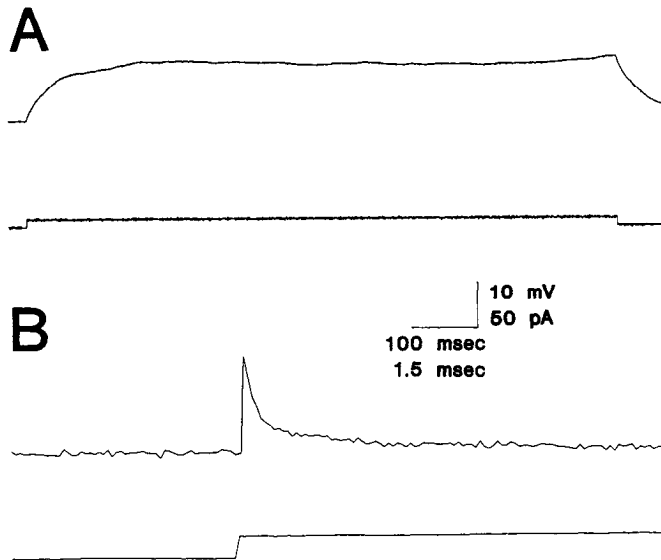
The current–voltage relation for the complete set of transient inward currents, measured at the response peak, is shown in Figure 4B. The current began to activate at potentials more positive than −40 mV and reached a maximum of 739 pA near

Table 2. Composition of electrode solutions (in mM)

Component	A Control (10^{-7} M Ca)	B Control (10^{-9} M Ca)	C $I_{(K)}$ blockade (10^{-7} M Ca)	D $I_{(K)}$ blockade (10^{-9} M Ca)
KCl	116	116	0	0
CsCl	0	0	96	96
TEA-Cl	0	0	20	20
EGTA	2	10	2	10
HEPES	4	4	4	4
MgCl$_2$	0	2	0	2
CaCl$_2$	1.6	0.08	1.6	0.08

A

B

10 mV
50 pA
100 msec
1.5 msec

Figure 2. Measurements for electrical membrane constants and series resistance. *A, Upper trace* shows voltage response to a 10 pA step of current shown in *lower trace*. The time constant, determined from the voltage response, is 20 msec. Plateau voltage was 13.4 mV, giving an input resistance of 1.34 GΩ and membrane capacitance of 15 pF. *B*, Determination of electrode series resistance. Capacitive transient recorded under voltage clamp (*upper trace*) in response to a 5 mV step (*lower trace*). Time constant was 0.15 msec. With membrane capacitance of 15 pF, calculated series resistance was 10 MΩ.

A

-75
-40
-35
-30
-25
-20
-15

200 pA
40 mV
8 msec

B

Current (pA)
0
-40
-80

-175   -125   -75
Vcommand (mV)

200 pA
40 mV
8 msec

-75
-90
-110
-130
-150
-170

Figure 3. Whole-cell currents. *A*, Responses to depolarizing voltage steps. Holding potential was −75 mV. Electrode solution A; bathing solution A. In this and subsequent figures, the *upper traces* are current responses and *lower traces* show time course and magnitude of voltage steps. Numbers near traces indicate the voltage to which the membrane was stepped. The capacitive and leak currents were mostly eliminated by subtraction of control records, but transients at the onset and offset of the current traces are remnants of the capacitive currents. *B*, Responses to hyperpolarizing voltage steps. *Inset, I–V* relation for hyperpolarizing steps. Measurements taken at the time indicated by the solid square in upper trace. Straight line is a least-squares fit. The input resistance was 1.1 GΩ. Same cell used in *A* and *B*.
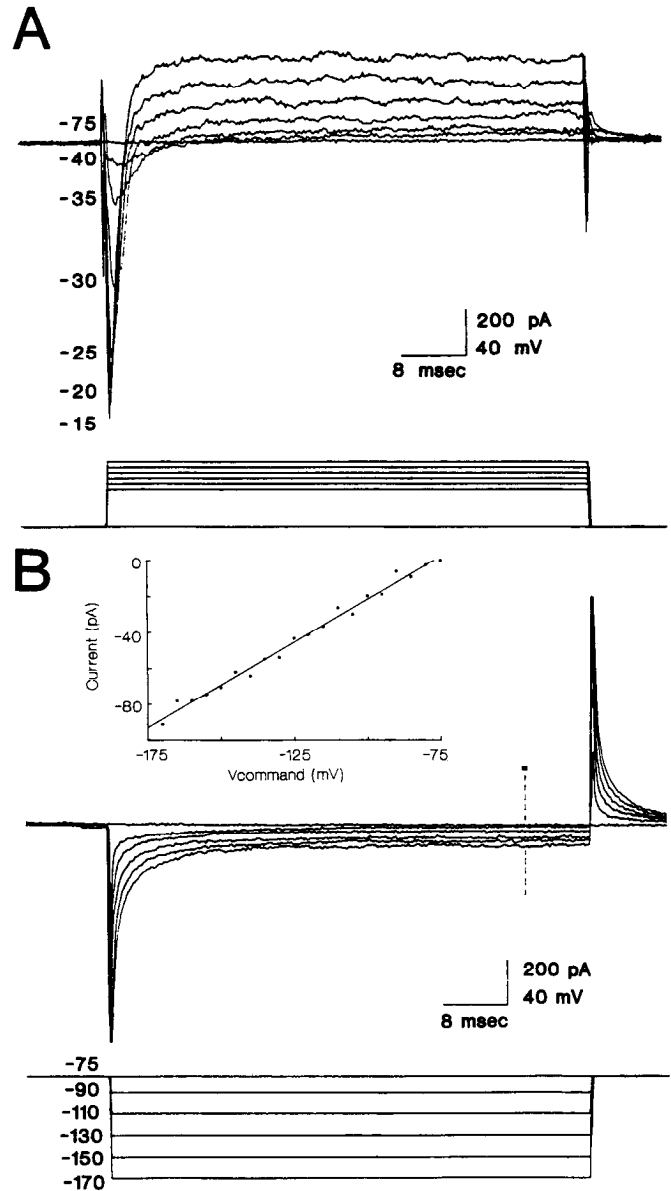
−15 mV, similar to that of other membranes (Cole and Moore, 1960; Lasater, 1986; Lipton and Tauck, 1987). The reversal potential for this current was near +45 mV. Table 4 summarizes the statistics for the whole-cell inward current data for all cells studied.

Inactivation of transient inward current. Inactivation of the transient inward current was measured in the conventional way by preceding a fixed magnitude depolarizing test pulse to −10 mV with a series of conditioning pulses to potentials ranging from −80 to −15 mV (Hodgkin and Huxley, 1952a, b). Figure 5*A* shows the currents elicited following these conditioning steps, and Figure 5*B* shows the inactivation curve derived from these measurements.

In 8 cells, inactivation began at potentials more *positive* than −65 mV and was nearly complete at −25 mV. For potentials more positive than −35 mV, the conditioning steps themselves entered the activation range, and inactivation was therefore overestimated. The inactivation range is very similar to that found in rat (Lipton and Tauck, 1987).

The transient inward current was eliminated by 0.33 μM or more TTX (solution D) (Moore et al., 1967). These observations, along with the measured reversal potential of +45 mV, are consistent with the notion that the transient inward current is carried by sodium.

Sustained inward currents. A sustained inward current, elicited by depolarizing voltage steps, could be measured by block-

ing the outward currents with 96 mM cesium and 20 mM TEA in the recording electrode and by blocking the sodium current with TTX in the bathing solution. Of the 24 cells studied, activation began between −45 and −30 mV. Selected currents

←

Figure 1. Photomicrograph of a retinal slice in which the axon was allowed to take up rhodamine before dissection (see Materials and Methods). In this and 12 other retinas examined, almost all ganglion cells were stained, and very few cells in the inner nuclear layer were ever stained. This suggests that most cells at the inner margin of the retina are ganglion cells (have axons) and that virtually no cells in the inner nuclear layer are ganglion cells. The observation verifies our assertion that the measurements both in slices and isolated cells were taken from ganglion cells. The slice was transilluminated with green light and epiilluminated and viewed through a 580 nm barrier filter, giving the rhodamine cells an orange appearance.
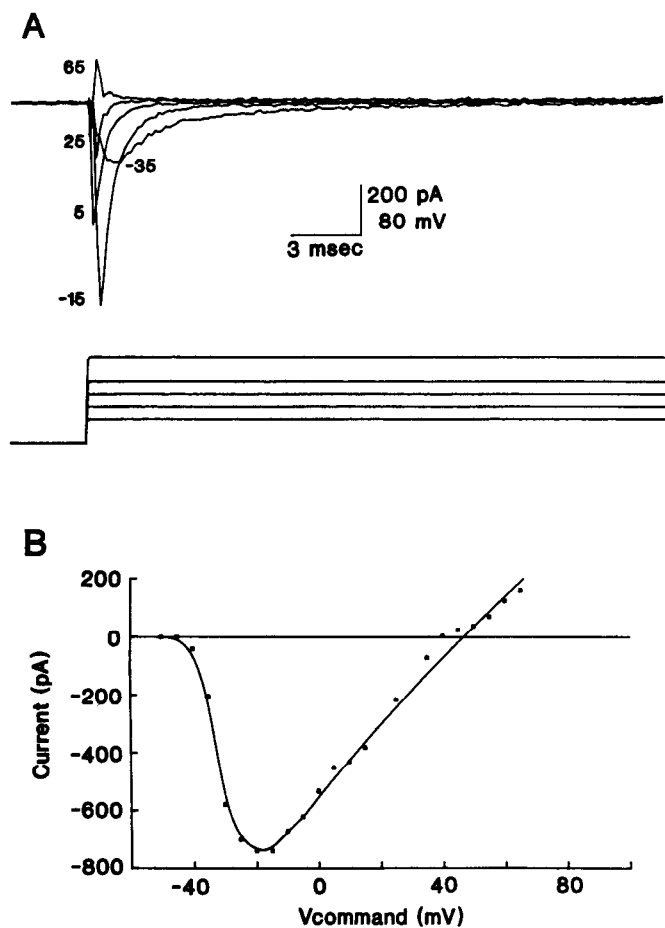
A

B

Figure 4. *A*, Isolation of the inactivating inward current. Holding potential was −75 mV. Cs/TEA (solution D) was used in electrodes and bathing solution contained 2 mM Co (solution B). Capacitive and leak currents were subtracted. *B*, Current–voltage relation for inactivating inward current. Points measured at response peak for every 5 mV voltage increment.

from a typical cell are shown in Figure 6*A* for a cell held at −75 mV and stepped to the indicated potentials.

The current–voltage relationship, measured at the peak response, for the complete set of voltage steps is shown in Figure 6*B*. The current began to activate at −35 mV and reached a maximum of 280 pA near −5 mV, similar to that described for
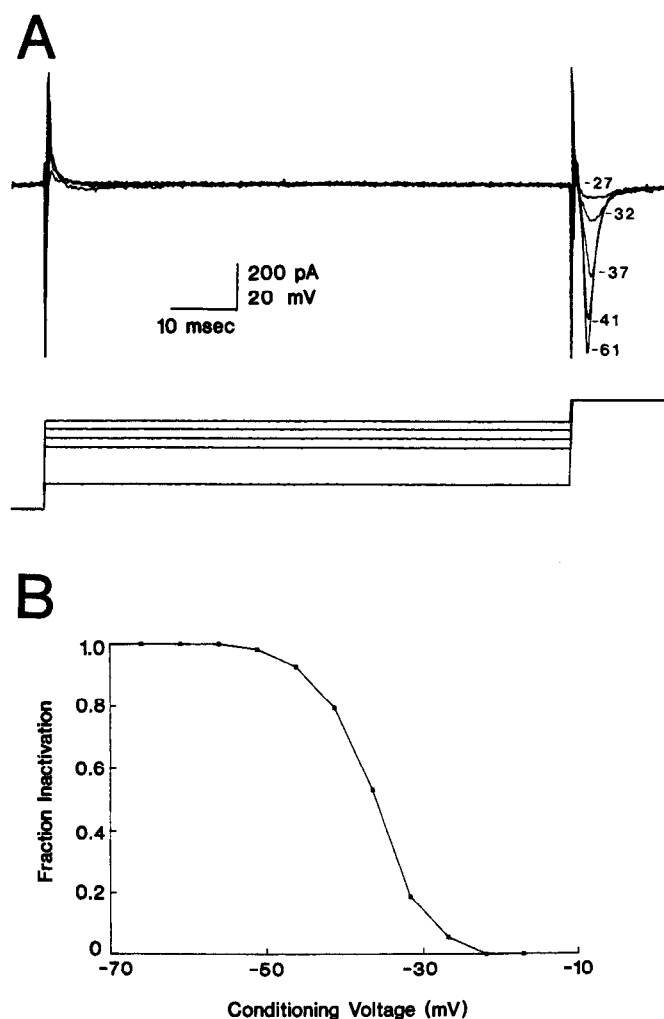
A

B

Figure 5. Inactivation of inward current. *A*, Response currents. Holding potential was −75. Cs/TEA electrode solution D was used and Ringer contained 2 mM Co and no added Ca (solution B). Capacitive artifacts and leak currents were not subtracted. *B*, Inactivation curve for cell in *A* given as the fraction of maximal current (measured at peak) versus the magnitude of the conditioning voltage.

other retinal cells (Kaneko and Tachibana, 1985; Lasater, 1986; Lipton and Tauck, 1987). For potentials more positive than −5 mV, the current decreased. Statistics for other cells are compiled in Table 4.

Table 3. Whole-cell data

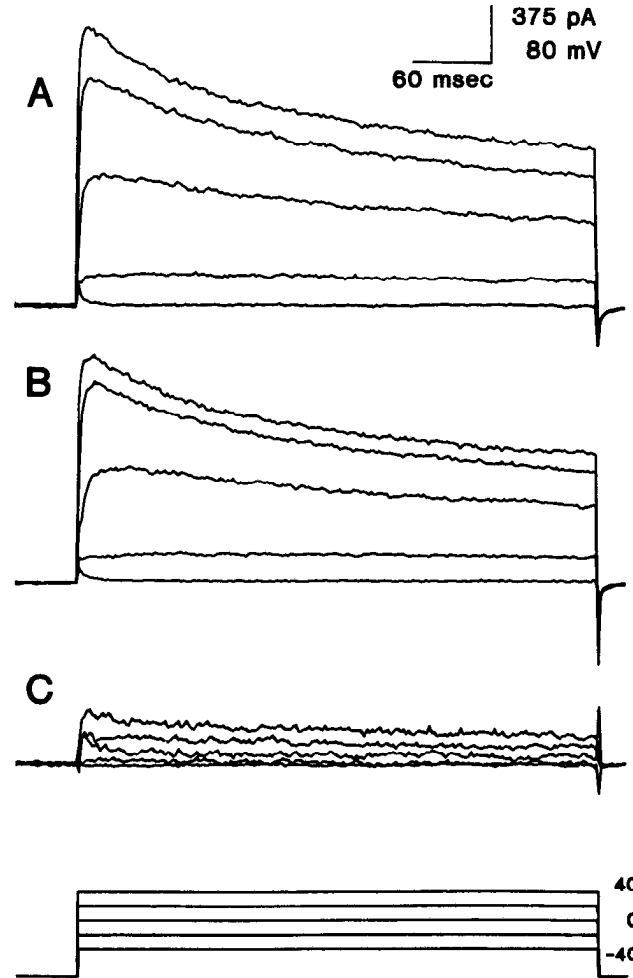| Parameter	Range	n	Mean	SEM
Sodium activation				
Beginning of activation (mV)	−40 to −29	16	−37.6	0.45
Peak current voltage (mV)	−20 to −5	15	−12.8	1.26
Peak current amplitude (nA)	−0.84 to −2.2	14	−1.32	0.13
Potassium activation				
Beginning of activation (mV)	−39 to −28	15	−33.1	1.05
Amplitude at −15 mV (nA)	0.111–0.966	15	332.7	53.1
Passive membrane properties				
Input resistances (GΩ)	0.878–10	33	2.9	0.39
Membrane capacitance (pF)	9–40	15	21.25	2.26
Membrane time constants (msec)	18–52	15	41.3	3.04
Resting levels (mV)	−52 to −91	41	−67.5	1.5
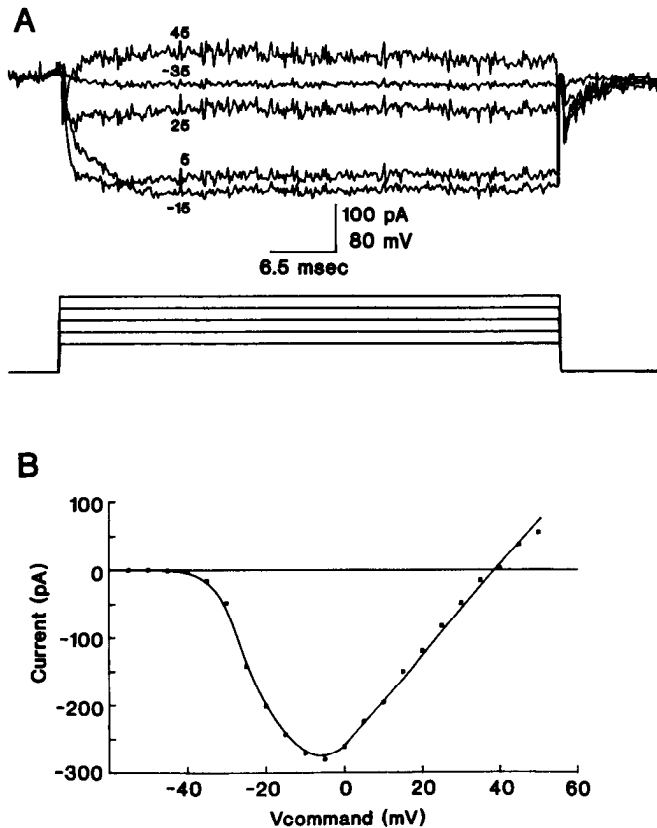
Figure 6. Isolation of the calcium current. A, Sustained inward currents. Cs/TEA electrode solution D was used and Ringer contained 1 μM TTX (solution C). Capacitive and leak currents were subtracted. Noise at more positive potentials was due to scaling and subtracting small responses in control steps. B, Current-voltage relation for the sustained inward current for cell in A. Current was maximal at −5 mV and reversed near +40 mV.

The reversal potential for this current was near 40 mV and is similar to that reported by others (Fenwick et al., 1982; Lee and Tsien, 1982; Lipton and Tauck, 1987). The reversal potential is more negative than the calculated reversal potential for the calcium current, possibly because of an outward current carried by cesium or other ions through the calcium channels.

The sustained inward current inactivated very slowly, with time constants between 3.3–1.3 sec for voltage steps ranging from −30 to −5 mV, respectively. This current decreased in magnitude or "ran down" over a period of 5–10 min during a sequence of measurements.

Figure 7. Cobalt-blocked components of outward currents. A, Total outward currents. Responses to potentials indicated by the stimulus traces. Holding potential was −80 mV. KCl electrode solution B was used and Ringer contained 1 μM TTX (solution C). B, Outward current responses in the presence of 2 mM Co and no added Ca (solution D). Same potentials as in A. C, Measured calcium-dependent outward currents determined by subtracting the currents in B from the total outward currents in A. This record is an underestimate of the full potassium current because a component of calcium current (Fig. 6) also exists. The calcium-activated potassium currents are sustained, and the calcium currents are relatively sustained, inactivating very slowly (see text).

This current was blocked by Co^{2+} (1–4 mM; see Fig. 4A) (Weakly, 1973) but was unaffected by TTX or choline substitution. These observations and the reversal potential near +40 mV suggest that it is carried primarily by calcium.

Table 4. Inward currents

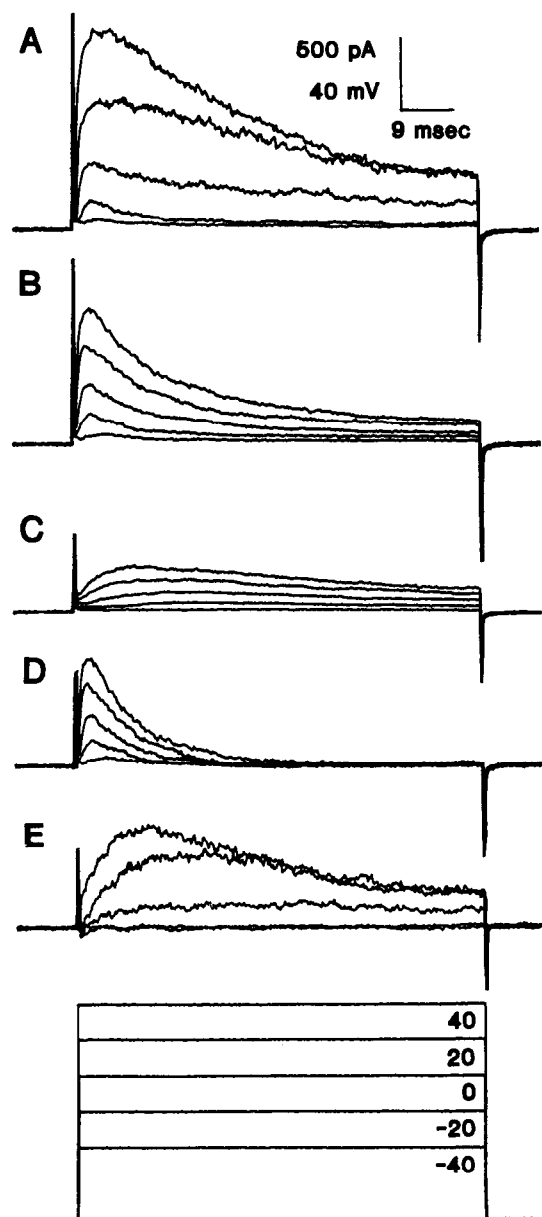| Parameter	Range	n	Mean	SEM
Transient inward currents				
Beginning of activation (mV)	−45 to −30	21	−37.9	0.79
Peak current voltage (mV)	−20 to −3	21	−12.4	1.34
Maximum current (nA)	−0.329 to −2.2	19	−0.968	0.123
Half inactivation voltage (mV)	−38.3 to −44	8	−41.5	0.63
Sustained inward currents				
Beginning of activation (mV)	−45 to −23	24	−34.7	0.79
Peak current voltage (mV)	−5 to 17	23	4.4	1.56
Maximum current (nA)	−0.17 to −0.5	23	−0.326	22.7

Figure 8. Separation of I_A current with 4AP. *A*, Outward currents in the presence of TTX and Co^{2+} (solution D). *B*, Currents in the presence of TTX, 20 mM TEA, and Co^{2+} (solution E). *C*, Currents in the presence of TTX, TEA, Co^{2+}, and 2 mM 4AP. *D*, The difference representing the 4AP-blocked current I_A. *E*, The TEA-sensitive current (A-B).

Composite outward currents. The full complement of outward currents elicited by depolarizing voltage steps is shown in Figure 7*A*. The transient inward current was blocked with TTX in the bath. Currents were activated by steps more positive than −40 mV. They peaked and then slowly decayed to a plateau level.

These composite currents were separated into 4 components. In the order of decreasing rates of inactivation these are (1) a rapidly inactivating current ($\tau \leq 30$ msec) resembling the I_A of Conner and Stevens (1971a, b); (2) a more slowly inactivating current ($\tau = 200$–400 msec) labeled I_B here; (3) a very slowly inactivating current ($\tau = 2$–5 sec) labeled I_C here; and (4) a sustained calcium-activated component, $I_{K(Ca)}$. We were able to measure each of these currents separately as shown below.

The calcium-activated current: $I_{K(Ca)}$. The calcium-activated

Table 5. Outward current statistics

Parameter	Range	n	Mean	SEM
Reversal potential for tail currents (mV)	−76 to −93	4	−85	4.2
Outward current magnitude at +10 mV (nA)	0.381–1.9	25	0.954	0.066
Dissection of total outward current Cobalt-blockable current at +10 mV (nA)	0.075–0.678	16	0.265	0.052
I_B at +10 mV (nA)	0.23–1.01	14	0.571	0.07
I_C at +10 mV (nA)	0.184–0.550	14	0.342	0.029

component of the outward current (Meech and Standen, 1975) was determined by subtracting the currents measured in the presence of 2 mM Co^{2+} and 0 mM Ca^{2+} (as shown in Fig. 7*B*) from the complete currents (shown in Fig. 7*A*). The difference is shown in Figure 7*C*. This current appears to be sustained at all potential levels. Because the calcium-activated potassium current is offset by a steady calcium current, the magnitude of the outward component shown here is an underestimate of the true value.

Fast inactivating current: I_A. The fastest transient component of the outward current was blocked by 1–2 mM 4-AP (Thompson, 1977; Lipton and Tauck, 1987). This current was revealed by subtracting records taken in the presence of 4-AP from those in its absence. Figure 8*A* shows the total outward current in the presence of 2 mM Co^{2+} and TTX (solution D). Figure 8*B* shows currents measured in the presence of Co^{2+}, TTX, and 20 mM TEA (solution E). Figure 8*C* shows currents measured in the presence of Co^{2+}, TTX, TEA, and 2 mM 4-AP. Figure 8*D*, the difference between the outward currents measured in the presence of 4-AP (Fig. 8*C*) and its absence (Fig. 8*B*), reveals a current with very short time course, less than 15 msec.

This rapidly inactivating current was not present in all cells, and in some cells a slower current was also blocked by 4-AP (Hermann and Gorman, 1981).

The TEA-sensitive component of the outward current is shown in Figure 8*E*, derived by subtracting the currents measured in the presence of TEA (Fig. 8*B*) from those in its absence (Fig. 8*A*). The more slowly inactivating outward currents described below were TEA sensitive.

More slowly inactivating outward currents: I_B and I_C

In the presence of cobalt and TTX, 2 additional, more slowly inactivating outward currents remained. They are shown, on a slower time scale, by the dotted trace in Figure 9*A*. Their decay could be approximated by a pair of exponentials. The time constants for the exponentials were determined by first fitting the slow component of the decay using the last 1000 msec of the trace. This slow exponential ($\tau = 4.03$ sec) was then peeled away from the original trace, leaving another exponential that could be fitted with a faster time constant ($\tau = 339$ msec).

The solid line in Figure 9*A*, composed of these 2 exponentials, provides an excellent fit to the original trace. The time courses for the decay of the 2 exponential current components, the slow component (dots) and faster component (crosses), are shown separately in Figure 9*B*.

The total outward currents recorded in the presence of TTX and Co are shown in Figure 10*A*. 4AP reduced the time to peak

A

250 pA
80 mV
450 msec

B
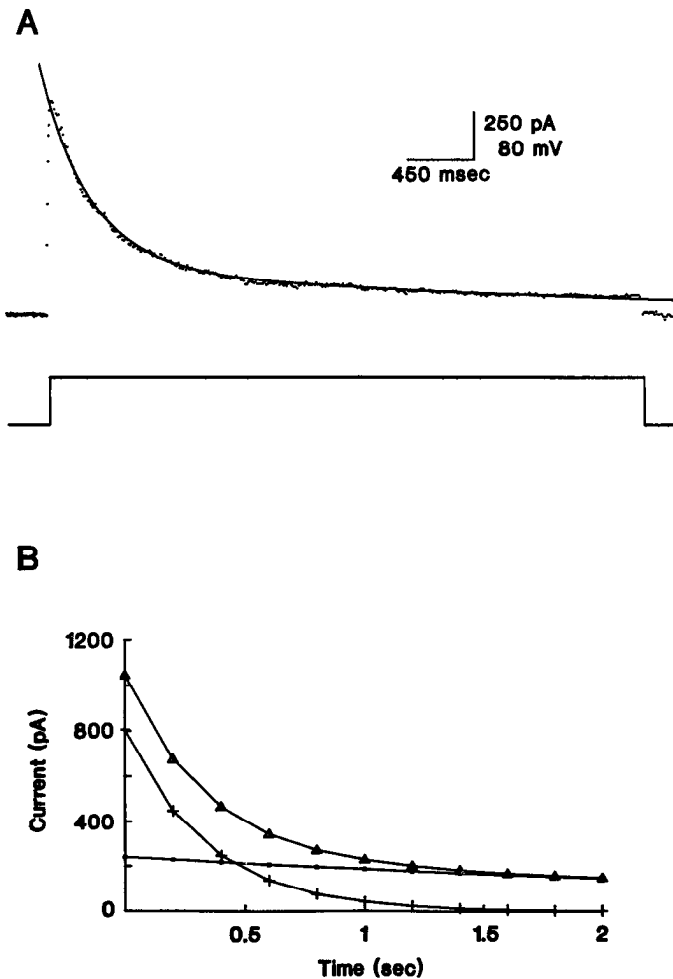
Figure 9. Double-exponential fit of slowly inactivating outward currents I_B and I_C. *A, Dotted trace* is the outward current in response to a step to 0 mV in the presence of TTX and Co^{2+}. Holding potential was −80 mV. *Solid line* is the best double-exponential fit. τ_B was 339 msec and τ_C was 4.03 sec. *B,* The time course of decay for the total (*open triangles*), I_B (*crosses*), and I_C (*dots*) outward current components.

for these currents, so the rise time in Figure 10*B* is slower than in Figure 10*A*, due to the blockade of I_A. 4AP did not affect the more slowly decaying currents (Fig. 10*B*) and the remaining current in 10*B* resembles that of Figure 10*A*. I_C, the most slowly inactivating current, was isolated by inactivating I_B with a 1.2 sec conditioning pulse to 0 mV (Fig. 10*C*).

The slowly inactivating outward currents, I_B and I_C, were isolated by taking advantage of the large disparity in their time constants of inactivation. We showed in Figure 9 that at 1.2 sec I_B is almost completely inactivated. The magnitude I_C is, however, underestimated since it is slightly inactivated at 1.2 sec (see below). I_B was obtained by subtracting I_C (Fig. 10*C*) from the currents that remained in the presence of Co and 4AP (Fig. 10*D*).

Voltage-dependent inactivation of I_B

The voltage-dependence of *inactivation* of I_B was measured in the conventional way by preceding a depolarizing test pulse from −80 mV to +10 mV with conditioning pulses to different potential levels as shown in Figure 11*A*. It was important to determine the optimum duration for the conditioning pulse used to inactivate I_B since the measurement could be contaminated


500 pA
80 mV
60 msec

A

B

C

D

40
20
0
-20

0

-80
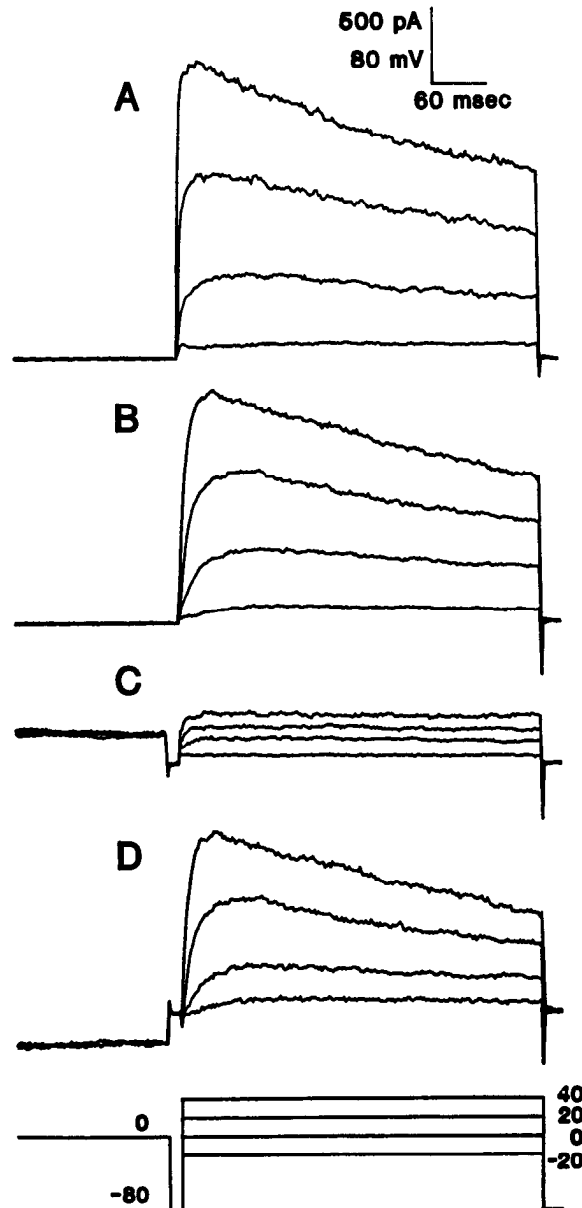
Figure 10. Separation of slowly inactivating currents, I_B and I_C. *A,* Outward current responses to the potentials indicated by the stimulus traces. The membrane was held at −80 mV. KCl electrode solution B was used, and the Ringer contained 1 μM TTX, 2 mM Co, and no added Ca (solution D). All outward currents except $I_{K(Ca)}$ are present. *B,* Responses after 1 mM 4AP was added to the bath. 4AP blocked a sustained component of the outward current in addition to I_A. *C,* Responses after 0 mV conditioning level for 1.2 sec prior to the voltage steps. These conditions eliminate I_B. *D,* Transient outward current I_B alone, determined by subtracting the sustained outward currents I_C in *C* from the composite outward currents in the presence of 4AP (*B*).

by I_C, which also inactivates, albeit much more slowly. The optimal duration for the conditioning pulse used to inactivate I_B should inactivate as much of I_B, but as little of I_C, as possible. This duration can be found from the solution of the equation:

$$\frac{d}{dt}[(e^{-t/\tau B}) - (e^{-t/\tau C})] = 0, \qquad (1)$$

where τ_B and τ_C are the inactivation time constants for the fast and slow components, respectively. The quantity in brackets is

A

B
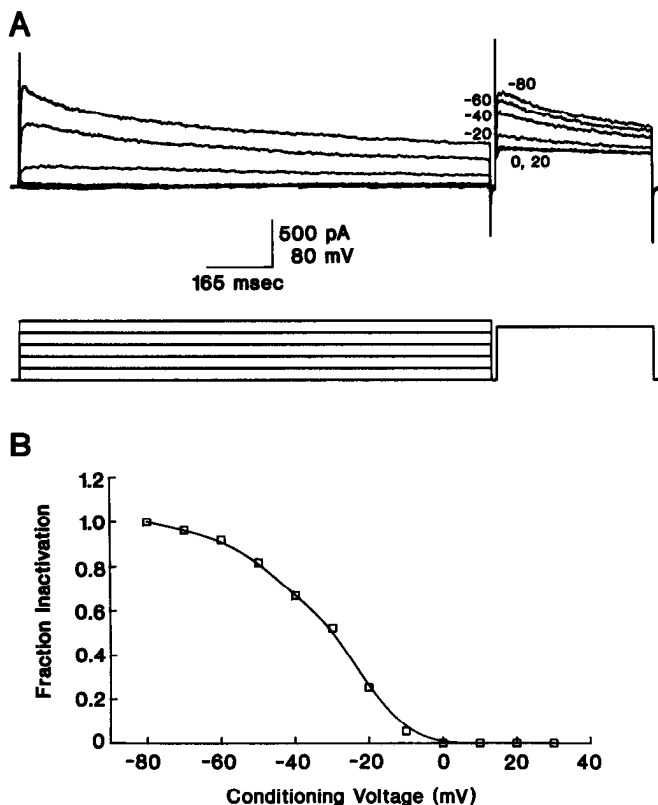
Figure 11. Inactivation of I_B. *A,* Current responses to a test pulse to +10 mV preceded by conditioning pulses to different potentials as indicated near the responses. KCl solution B was used and the Ringer contained 1 μM TTX and 2 mM Co but no added Ca (solution D). *B,* Inactivation curve for I_B. The percentage of the peak maximum outward current was plotted as a function of the magnitude of the conditioning pulse at 30 msec, a time at which I_A was fully decayed (see Fig. 9).

the difference in the fraction of the 2 remaining components as a function of time. When its derivative (in time) is zero, that difference is greatest. The solution to equation (1) is

$$t = \tau_C\tau_B/(\tau_C - \tau_B)[\ln \tau_C - \ln \tau_B]. \tag{2}$$

Equation 2 predicts that, for a step to 0 mV, the difference between the remaining magnitudes of I_B and I_C will be greater than 71% between 0.7 and 1.2 sec.

We measured the inactivation range of I_B with a conditioning pulse of 1.2 sec duration, when 3% of I_B and 74% of I_C remained for a fully inactivating conditioning pulse, as shown in Figure 9B. We were able to measure the changes in magnitude of I_B after conditioning pulses to different potential levels by stepping to +10 mV but measuring the current 30 msec later to allow I_A ($\tau \le 20$ msec) to decay. Inactivation of I_B was very broad, spanning the potential range from -80 to 0 mV (Fig. 11B).

Reversal potential for outward currents. We determined the reversal potential for the outward current from the sign and magnitude of the decay of the fully activated currents measured at different potential levels as shown in Figure 12. Calcium currents, which could offset the outward current reversal potential, were eliminated with 2 mM Co^{2+} replacing calcium in the bathing medium. This also eliminated one component of the outward current, $I_{K(Ca)}$.

The membrane was held at -80 mV and first stepped to 0 mV, where a significant fraction of the current was activated; then it was stepped to potentials between -55 and -110 mV. Figure 12A shows some selected currents, and Figure 12B shows the current–voltage curve using currents measured at all steps. The reversal potential derived from the least-squares fit is -77 mV. Similar results were found in 3 additional cells (-85 mV mean; see Table 5).

These currents were blocked by internal cesium and TEA, which suggests that they were potassium currents. The measured reversal potential at -77 mV is more positive than the calculated Nernst potential for potassium of -100 mV, possibly because the potassium channels are relatively nonselective.

A

B
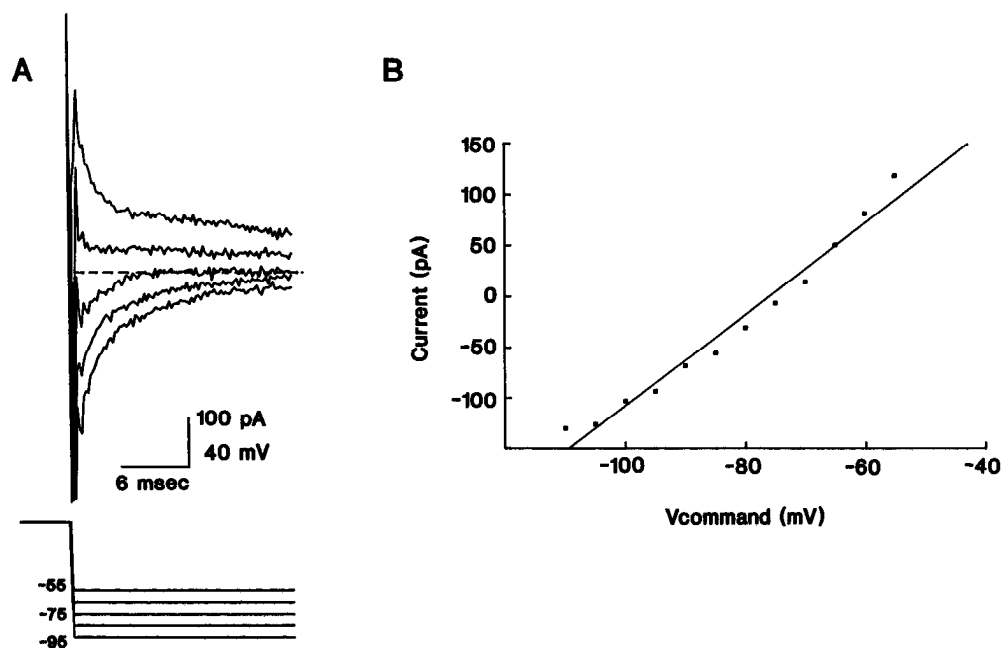
Figure 12. Reversal of the potassium tails. *A,* The membrane was held at -80 mV, then stepped from 0 mV in successive records to -110 to -55 in 5 mV increments. KCl electrode solution B was used and Ringer contained 1 μM TTX and 2 mM Co (solution D). Measurements were made 5.4 msec after the end of the step to avoid the capacitive transient. *B,* Current–voltage relation for currents for all steps over the full range of potentials. Tails reversed at -77 mV.
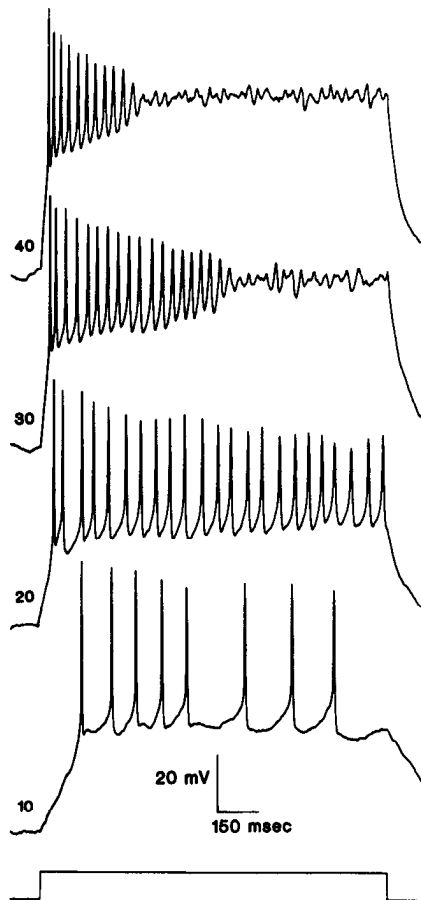
Spike activity in response to current steps

The presence of the inactivating current, I_B, suggests that its role in modulating the spike output of ganglion cells might be manifest in a membrane potential change with similar time constant. We looked under current clamp at the spike activity, and identified a slow depolarization of the membrane with time course similar to that of I_B. Then we eliminated other currents to confirm that these slow changes in spiking were mediated by I_B.

For relatively large input currents the spike train was terminated before the end of the current step. Figure 13 shows the normal spike train elicited at a series of current steps of increasing magnitude. With 10 pA of current the membrane was steadily depolarized and a series of spikes of relatively constant interspike interval was generated for the duration of the current step. With a 20 pA step, the spike frequency increased, and the membrane potential and spike rate were relatively sustained for the duration of the step. However, at 30 pA the spike train was truncated after about 500 msec and the membrane potential became gradually more positive during the step. For a 40 pA step the spike train was truncated even earlier.

The I_B current underlies slow membrane potential changes

The membrane currents for steps to -30, -20, and -10 mV were fit over the first 300 msec with exponentials. These cur-

rents, taken from the same cell as in Figure 13, had time constants of 240, 270, and 350 msec, respectively, as shown in Figure 14. These are consistent with the 339 msec time constant taken from the step to 0 mV shown in Figure 9.

We show that I_B underlies these currents by eliminating each of the other voltage-gated current components as shown in Figure 15. Figure 15*A* shows the normal spike activity elicited by a 30 pA current step. Figure 15*B* shows the behavior of the spike train in the presence of 4AP (I_A blocked). 4AP *decreased* spike frequency, an effect different from that predicted by Conner and Stevens (1971a, b). In many cases, I_A does not play a significant role in *truncating* spike activity. When the spiking was blocked with TTX, as in Figure 15*C*, the gradual membrane depolarization during the course of the current step became more apparent. Blocking the calcium current with Co^{2+} did not affect this gradual depolarization during the step as shown in Figure 15*D*. A relationship between the exponential change in I_B shown in Figure 14, and the exponentiallike change in potential in Figure 15 is derived in the Discussion.

Discussion

Roles of inactivating outward currents. A variety of inactivating outward currents with different inactivation time constants, potential ranges, and pharmacological sensitivities have been described earlier. The fastest of these, I_A, has been implicated as a factor modulating spike *frequency* by Conner and Stevens (1971a) and Adams et al. (1982). This current, with time constant between 5 and 100 msec, depending upon preparation, has been identified by its sensitivity to 4AP and has been found
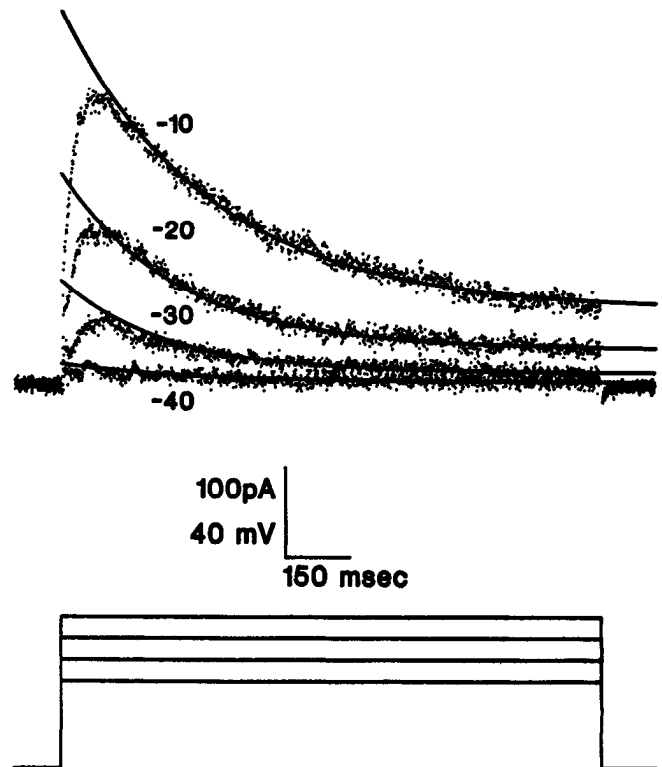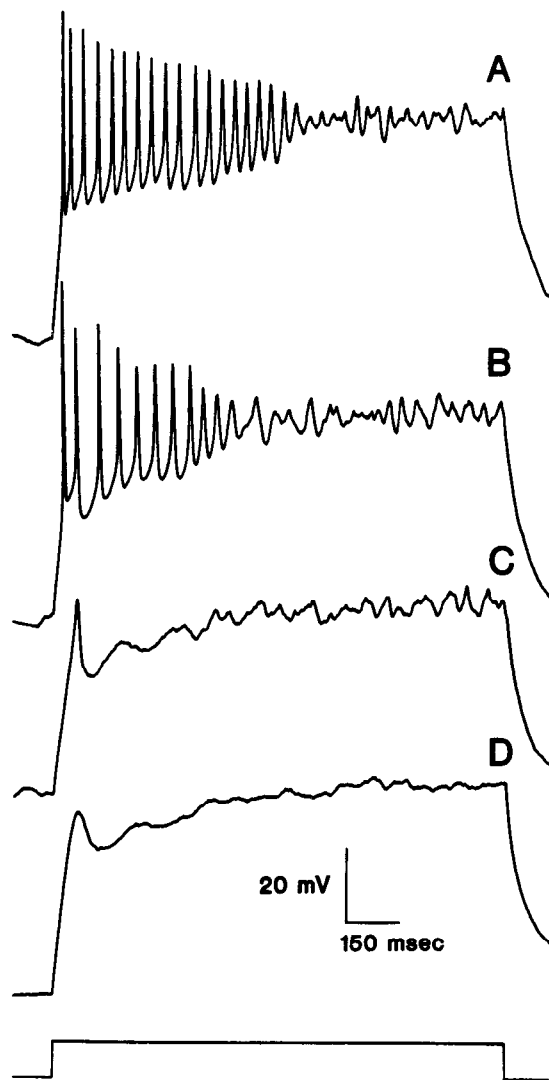

Figure 13. Spike activity at different input current magnitudes. Current step magnitudes in pA are shown to the left of each trace. KCl solution B was in the electrode and control Ringer (solution A) was in the bath. Spike rates are constant for 10 and 20 pA steps, but spikes are truncated as the membrane potential rises to more positive levels for 30 and 40 pA steps.

Figure 14. Fitting I_B currents with exponentials. Records taken in the same cell as in Figures 13 and 15. Measurement made in the presence of 2 mM Co^{2+}, 1 μM TTX, and 2 mM 4AP. Fits were made over the first 300 msec after the peak. The time constants for these curves were 240 msec at -40 mV, 250 msec at -30 mV, 270 msec at -20 mV, and 330 msec at -10 mV. These fits suggest that I_B is a single-exponential current with a distinct time course at each potential.

by us in tiger salamander and by Lipton and Tauck (1987) in rat ganglion cells.

A second class of inactivating outward current, lacking 4AP sensitivity and having slower kinetics and activation ranges, has been described by Aldrich et al. (1979) (also see Adrian et al., 1970). This corresponds more closely to the current I_B described here. Finally, a much more slowly inactivating outward current was described by Schwartz and Vogel (1971) with time constant between 600 msec and 3.5 sec. This may be similar to the very slowly inactivating outward current, I_C, described here.

I_B is responsible for the depolarizing shift in membrane potential

I_B appears to be responsible for the slow rise in potential following a steady input current as shown in Figure 15D. The
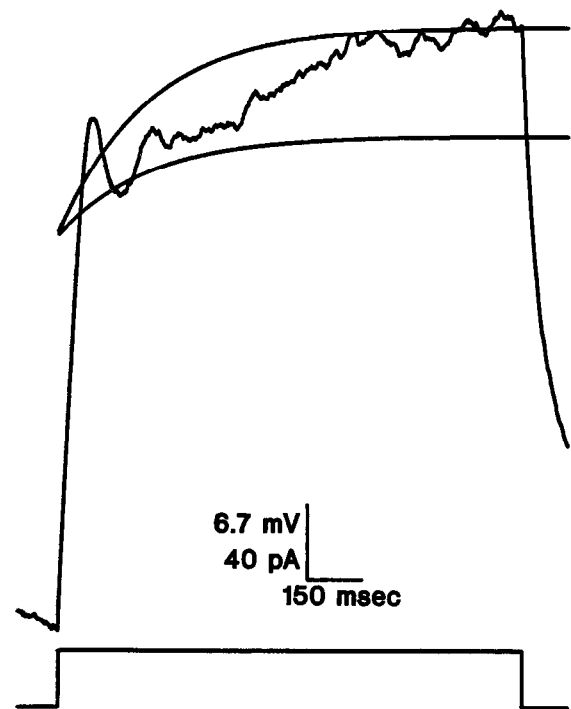
association between I_B and the rise is supported by the finding that the time constant for the underlying currents shown in Figure 14 and that of the potential rise are quite similar (Fig. 15D).

Although the actual rise in potential in Figure 15D cannot be fit by an exponential, when the change in membrane slope conductance underlying the inactivation of I_B itself is taken into account, the role of I_B in mediating the potential change is strongly supported.

The rise in *potential* could not be fit with an exponential because the input slope resistance of the cell increases from 0.25 to 0.52 GΩ during the change in potential. This conductance decrease of 2.08 nS is due almost entirely to the inactivation of I_B since most other voltage-dependent potassium conductances have been blocked and I_C, being much slower, has not changed sufficiently during this interval. In fact, the conductance change calculated from the transient current I_B between -40 and -20 mV, assuming a reversal potential for potassium near -80 mV, is also about 2 nS. In Figure 16 we were able to *straddle* the potential rise during the step by using 2 I_B exponentials, with 240 msec time constant but differing in magnitude to take into account the change in chord conductance: The lower exponential is the voltage using the initial input resistance of 0.25 GΩ, and the upper exponential is that using the final input resistance of 0.52 GΩ. The time constant changes only from 240 to 270 msec over this potential range, so the fit using a time constant of 240 msec is a reasonable approximation. These curves show that

Figure 15. Membrane potential in absence of voltage-gated currents. KCl solution B was used in the electrode. *A,* Normal spike response to a 30 pA step. *B,* I_A is eliminated in the presence of 2 mM 4AP. Spike activity decreases and membrane potential becomes more positive. *C,* Spiking is blocked in TTX, but membrane potential continues to increase during the step. *D,* In Co^{2+} calcium, current is blocked, but the membrane potential rise is unaffected. I_B and upward change in potential remain intact in all records, suggesting a correlation. Same cell as Figure 13.

Figure 16. Fitting the slow membrane polarization with the time course of I_B. The gradual membrane depolarization measured in Figure 15D is compared with the magnitude and kinetics of I_B measured in Figure 14. We used currents with a time constant of 240 msec, the time constant for the current at -30 mV. The *lower* and *upper* curves represent the voltage due to this current through the chord resistance at the beginning (0.25 GΩ) and end (0.52 GΩ) of the trace, respectively. It is likely that no other significant conductances contribute to the chord resistance during the inactivation (see text).

even though the voltage change cannot be fit by a single-exponential function, it can be bracketed using 2 exponentially decaying currents that take into account the change in chord resistance of the cell during the voltage excursion.

Functional significance of I_B. I_B appears to serve at least 2 important functions. First, when I_B is activated rapidly by excitatory currents large enough to elicit spike activity, it acts to shunt the membrane, thereby limiting depolarization to a level of little sodium inactivation, assuring that more than a single spike will be generated. Second, the gradual inactivation of this current with time will limit the number of spikes that a ganglion cell generates by allowing depolarization into the sodium inactivation region. Thus, I_B seems (1) to extend the graded range of response in terms of spike number for short periods of up to 200 msec following a large excitatory input and (2) to limit the total number of spikes generated by the cell.

These findings suggest for the first time that the ganglion cell membrane contains voltage-gated currents that act to limit the time course of the spike response. Such modulations have previously been assigned to lateral interactions (Werblin, 1978) or voltage-gated currents (Attwell and Wilson, 1980) in distal regions of the retina. In future work we hope to be able to assign this and other functions to specific classes of ganglion cells.

References

Adams, P. R., D. A. Brown, and A. Constanti (1982) M-Currents and other potassium currents in bullfrog sympathetic neurones. J. Physiol. (Lond.) 330: 537–572.

Adrian, R. H., W. K. Chandler, and A. L. Hodgkin (1970) Voltage clamp experiments in striated muscle fibres. J. Physiol. (Lond.) 208: 607–644.

Aldrich, R. W., P. A. Getting, and S. H. Thompson (1979) Inactivation of delayed outward current in molluscan neurone somata. J. Physiol. (Lond.) 291: 507–530.

Attwell, D., and M. Wilson (1980) Behaviour of rod network in tiger salamander retina mediated by membrane properties of individual rods. J. Physiol. (Lond.) 389: 287–316.

Barnes, S., and F. Werblin (1986) Gated currents generate single spike activity in amacrine cells of the tiger salamander retina. Proc. Natl. Acad. Sci. USA 83: 1509–1512.

Baylor, D. A., and R. Fettiplace (1979) Synaptic drive and impulse generation in ganglion cells of turtle retina. J. Physiol. (Lond.) 288: 107–127.

Belgum, J. H., D. R. Dvorak, and J. S. McReynolds (1982) Sustained synaptic input to ganglion cells of mudpuppy retina. J. Physiol. (Lond.) 326: 91–108.

Belgum, J. H., D. R. Dvorak, and J. S. McReynolds (1983) Sustained and transient inhibitory inputs to on-off ganglion cells in the mudpuppy retina. J. Physiol. (Lond.) 340: 599–610.

Cole, K. S., and J. W. Moore (1960) Ionic current measurements in the squid giant axon membrane. J. Gen. Physiol. 44: 123–167.

Connor, J. A., and C. F. Stevens (1971a) Voltage clamp studies of a transient outward membrane current in gastropod neural somata. J. Physiol. (Lond.) 213: 21–30.

Connor, J. A., and C. F. Stevens (1971b) Prediction of repetitive firing behavior from voltage clamp data on an isolated neurone soma. J. Physiol. (Lond.) 213: 31–53.

Fenwick, E. M., A. Marty, and E. Neher (1982) Sodium and calcium channels in bovine chromaffin cells. J. Physiol. (Lond.) 331: 599–635.

Firestein, S., and F. Werblin (1987) Gated currents in isolated olfactory receptor neurons of larval tiger salamander. Proc. Natl. Acad. Sci. USA 84: 6292–6296.

Hamill, O. P., A. Marty, E. Neher, B. Sakmann, and F. J. Sigworth (1981) Improved patch-clamp techniques for high resolution current recording from cells and cell-free membrane patches. Pfluegers Arch. 391: 85–100.

Hermann, A., and A. L. F. Gorman (1981) Effects of 4-aminopyridine on potassium in a molluscan neuron. J. Gen. Physiol. 78: 63–86.

Hodgkin, A. L., and A. F. Huxley (1952a) The components of membrane conductance in the giant axon of Loligo. J. Physiol. (Lond.) 116: 473–496.

Hodgkin, A. L., and A. F. Huxley (1952b) The dual effect of membrane potential on sodium conductance in the giant axon of Loligo. J. Physiol. (Lond.) 116: 497–506.

Kaneko, A., and M. Tachibana (1985) A voltage-clamp analysis of membrane currents in solitary bipolar cells dissociated from Carassius auratus. J. Physiol. (Lond.) 358: 131–152.

Lasater, E. M. (1986) Ionic currents of cultured horizontal cells isolated from the white perch retina. J. Neurophysiol. 55: 499–513.

Lee, K. S., and R. W. Tsien (1982) Reversal of current through calcium channels in dialysed single heart cells. Nature 297: 498–501.

Lipton, S. A., and D. L. Tauck (1987) Voltage-dependent conductances of solitary ganglion cells dissociated from the rat retina. J. Physiol. (Lond.) 385: 361–391.

Lukasiewicz, P. D., and F. S. Werblin (1985) Electrical properties of tiger salamander retinal ganglion cells. Abstr. Soc. Neurosci. 11: 242.

Lukasiewicz, P., and F. S. Werblin (1986) Three different forms of ganglion cell activity mediated by synaptic and voltage gated currents. Invest. Ophthalmol. Vis. Sci. Suppl. 27: 130.

Meech, R. W., and N. B. Standen (1975) Potassium activation in helix asperso neurons under voltage clamp: A component mediated by calcium influx. J. Physiol. (Lond.) 249: 211–239.

Miller, R. F., and R. F. Dacheux (1976) Synaptic organization and ionic basis of on and off in mudpuppy retina. III. A model of ganglion cell receptive field organization based on chloride-free experiments. J. Gen. Physiol. 67: 661–678.

Moore, J. W., M. P. Blaustein, N. C. Anderson, and T. Narahashi (1967) Basis of tetrodotoxin's selectivity in blockage of squid axons. J. Gen. Physiol. 50: 1401–1411.

Schwartz, J. R., and W. Vogel (1971) Potassium inactivation using myelinated nerve fibres of Xenopus laevis. Pfluegers Arch. 330: 61–73.

Stewart, W. W. (1978) Functional connections between cells as revealed by a highly fluorescent naphthalimide tracer. Cell 14: 741–759.

Thompson, S. H. (1977) Three pharmacologically distinct potassium channels in molluscan neurones. J. Physiol. (Lond.) 265: 465–488.

Weakly, J. N. (1973) The action of cobalt ions on neuromuscular transmission in the frog. J. Physiol. (Lond.) 234: 597–612.

Werblin, F. S. (1977) Regenerative amacrine cell depolarization and formation of on-off ganglion cell response. J. Physiol. (Lond.) 264: 767–785.

Werblin, F. S. (1978) Transmission along and between rods in the tiger salamander retina. J. Physiol. (Lond.) 280: 449–470.

Wollner, D. A., and W. A. Catterall (1986) Localization of sodium channels in axon hillocks and initial segments of retinal ganglion cells. Proc. Natl. Acad. Sci. USA 83: 8424–8428.

Wunk, D. F., and F. S. Werblin (1979) Synaptic inputs to the ganglion cells in the tiger salamander retina. J. Gen. Physiol. 73: 265–286.